Numerical study on mountain waves generated by a two-dimensional mountain and their effect on the transport of Yellow Sand

Numerical Study on Mountain Waves Generated by a Two-Dimensional Mountain and Their Effect on the Transport of Yellow Sand*

Yoichi UTANOHARA**, Shigeo KIMURA*** and Takahiro KIWATA****

We have studied the effect of ground topography, focusing on mountain waves, on the transport of Yellow Sand by two-dimensional numerical simulation. An advection-diffusion equation for scalar concentration is solved to simulate the transport of Yellow Sand. Two different models are employed: the first is a one-layer model in which the density gradient is constant in the entire domain, and the other is a two-layer model in which the density gradient changes at an altitude of 11 km. In the both models stream lines at high altitude descend greatly toward the ground along the lee side of the mountain as the atmospheric stability increases. However, in the two-layer model, trapped mountain waves become stronger than those in the one-layer model, and rotors are also generated on the ground. These become stronger for larger mountain width, and the scalar concentration rapidly diffuses there. It is found that the ground scalar concentrations for the two-layer model are generally much larger, especially in the rotors, compared with those in the one-layer model.

Key Words: Mountain Waves, Rotor, Trapped Lee Waves, Stratified Flow, Yellow Sand, Computational Fluid Dynamics

1. Introduction

Yellow Sand is a sand transport phenomenon in East Asia, which originates from the Takla Makan Desert and the Gobi Desert in China. The soil in the desert is often blown up into the troposphere by strong surface winds and then transported by westerly winds to be deposited over East Asia. Yellow Sand phenomena are frequently observed during the spring season in Japan, and it is known that the dust comes in layers at heights between several hundreds meters and 5 km[1]. Of concern is that Yellow Sand deposition may cause damage to agriculture and stock-breeding, and that its radiative effect on the planetary heat balance is still not well understood. It has, however, also positive effects, such as neutralization of acid rain and nourishment of phytoplankton in the sea. Hence understanding the mechanism of the transport and the deposition of Yellow Sand is important for evaluating the environmental effects mentioned above.

Numerical modeling plays an important role in analyzing the transport mechanism of Yellow Sand. Several works have considered the long-range transport processes of Yellow Sand from the Asian continent to Japan[2]-[4]. There seem to be, however, no small-scale simulations that deal with local meteorology and topography in a range from several kilometers to several tens of kilometers, which is, we think, largely responsible for the deposition mechanism of dust at high altitude in troposphere.

Mountain waves are a typical small-scale meteorological phenomenon. They are generated on the leeward side of a mountain when the atmosphere is stably stratified; they grow stronger as the stability increases and often cause strong downslope windstorms[5]. With mountain waves, flows at high altitudes are often drawn downward behind the mountain. Hence, there is a possibility that mountain waves pull the Yellow Sand at high altitudes down to the ground. The main purpose of this study is to

* Received 16th March, 2006 (No. 06-4063)

** Institute of Nature and Environmental Technology, Kanazawa University, Kakuma-machi, Kanazawa-shi, Ishikawa 920–1192, Japan.
E-mail: utano@ryuko.ms.t.kanazawa-u.ac.jp

*** Institute of Nature and Environmental Technology, Kanazawa University, Kakuma-machi, Kanazawa-shi, Ishikawa 920–1192, Japan

**** The Graduate School of Natural Science and Technology, Kanazawa University, Kakuma-machi, Kanazawa-shi, Ishikawa 920–1192, Japan

apply a numerical simulation methodology to examine our hypothesis that mountain waves are responsible for Yellow Sand deposition.

2. Mathematical Formulation

Transient two-dimensional computations are performed using the commercial CFD software FLUENT. The governing equations are the continuity equation, the Navier-Stokes equation, and transport equations for density disturbance and scalar concentration. The Boussinesq approximation is applied to calculate a density-stratified flow[6),(7)]. The equations are

$$\frac{\partial(\rho u_i)}{\partial x_i}=0 \tag{1}$$

$$\frac{\partial(\rho u_i)}{\partial t}+\frac{\partial(\rho u_i u_j)}{\partial x_j} =-\frac{\partial p}{\partial x_i}+\frac{\partial}{\partial x_j}\left\{\mu_{eff}\left(\frac{\partial u_i}{\partial x_j}+\frac{\partial u_j}{\partial x_i}\right)\right\}-\delta_{ik}\rho g \tag{2}$$

$$\frac{\partial(\rho\rho')}{\partial t}+\frac{\partial(\rho u_i\rho')}{\partial x_i}=-\rho v\frac{d\rho_B}{dy} \tag{3}$$

$$\frac{\partial(\rho C)}{\partial t}+\frac{\partial(\rho u_i C)}{\partial x_i}=\frac{\partial}{\partial x_i}\left(\mu_{eff}\frac{\partial C}{\partial x_i}\right) \tag{4}$$

where the u_i is the velocity, especially v is the y-component velocity, μ_{eff} is the effective viscosity which is the sum of the molecular viscosity μ_m and the eddy viscosity μ_t, δ_{ik} is Kronecker's delta ($\delta_{ik}=1$ if $i=k$ and zero otherwise, and k indicates y-direction.), g is the acceleration due to gravity, C is the scalar concentration, ρ_B and ρ' are the background density and the perturbation density respectively, and $\rho=\rho_B+\rho'$ is used for the atmospheric density. The profile of the background density is assumed to be linear and given by

$$\frac{d\rho_B}{dy}=-N^2\frac{\rho_0}{g}, \tag{5}$$

where N is the Brunt-Väisälä frequency of an air parcel oscillating adiabatically in stratified fluid, and ρ_0 is the reference density. In this paper ρ_B at $y=0.5h_0$, where h_0 is the mountain height (see Eq. (7)), is used as ρ_0.

We use a standard $k-\epsilon$ turbulence model to evaluate the eddy viscosity. However, it should be emphasized that the main purpose of this study is to know how low Yellow Sand is pulled down by mountain waves. Turbulence is generally a much smaller scale phenomenon and has only a secondary effect on the mountain waves in the troposphere. In fact, vigorous turbulence cannot develop in stable atmosphere. On the contrary, once the dust comes into the atmospheric boundary layer, turbulent flow greatly prompts the diffusion process there.

The Froude number, Fr, given by

$$Fr=\frac{U}{Nh_0}, \tag{6}$$

is introduced as a parameter to indicate the atmospheric stability. The atmosphere becomes more stable as N increases, that is, Fr decreases. On the other hand, the atmosphere approaches a neutral state as Fr increases.

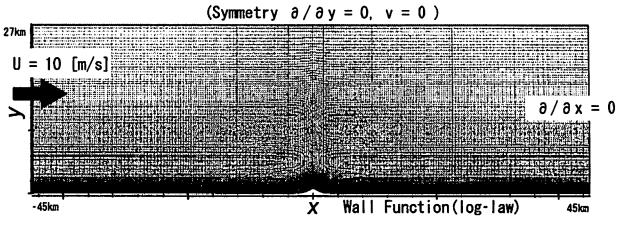

Fig. 1 Computational domain and boundary conditions

Figure 1 shows the computational domain and the boundary conditions. It covers a space −45 km~45 km in the x-direction and up to 27 km in the y-direction. Generally it is known that the height of tropopause is about 11 km and the computational domain we use here is much higher than that. The reason for this is to minimize the influence of numerical disturbances generated by wave reflections from the top boundary. A bell-shaped mountain known as "Witch of Agnesi", whose profile is given by

$$h(x)=\frac{h_0}{1+(x/a)^2} \tag{7}$$

is set at ground level in the middle of the domain; here $h_0=900$ [m] is the height of the mountain and $a=1\,000$ [m] is the half-width. In section 3.3 $a=500$ and 2 000 [m] are assigned for the half-width in order to investigate the effect of the mountain shape on flow patterns. The origin of the x- and y-axes is set on the ground at the center of the mountain. 251×201 grid points in x- and y-directions are employed when $a=1\,000$ [m], while 401×201 points are used for $a=500$ [m] and 251×201 points for $a=2\,000$ [m]. To obtain a finer resolution, grid points are closely spaced near the mountain and the ground. The boundary conditions are as follows: uniform velocity $U=10$ [m/s] at the inlet boundary, $\partial/\partial x=0$ at the outlet boundary, symmetry boundary ($\partial/\partial y=0$, $v=0$) at the upper boundary, and logarithmic velocity profile on the ground. An impulsive-start is used for the initial condition, which is a sudden acceleration of the flow from rest over the entire space. A time step of $\Delta t=1$ [s] is fixed for all the computations.

We employ two different atmospheric models: one is a one-layer model in which the density gradient is constant over the entire height; the other is a two-layer model in which the density gradient changes at an altitude of 11 km.

Yellow Sand is assumed to be released in layers of width 200 m at 10 km upstream from the mountain at altitudes of 1 and 2 km. The transport of Yellow Sand is simulated by an advection-diffusion equation for a passive scalar concentration (Eq. (1)). Gravitational settling is not considered[8]; this is due to the fact that, from observed data of Yellow Sand over Japan, the particle diameters are less than the order of several μm[9], hence the gravitational settling effect is negligibly small in the present problem. For the source of scalar concentration, the amount of emis-

sion per second for unit volume is set to $C_0 = 1\ [m^{-3}s^{-1}]$ in a 200 m × 200 m area.

The calculations are carried out by the finite volume method using the SIMPLE algorithm for pressure-velocity coupling. The time integration is done by an implicit second order accurate method. The convection term is discretized using the QUICK scheme, and the diffusion term is discretized by second-order central differences.

We validated our code by comparing our computational results with previously reported ones[8].

3. Results

3.1 One-layer model

Here the results for only $Fr = 1.0$ are shown and discussed, although we have found that other cases for different values of Fr are not so different from those for $Fr = 1.0$. In Figs. 2 and 3 we show the stream lines and the contour lines for the horizontal velocity at $t = 5\,000$ [s]. Mountain waves are an unsteady phenomenon so that they develop with time and propagate in the obliquely upward direction. Over the lee side of the mountain, the horizontal velocity becomes greater, which is a typical effect of mountain waves and is clearly seen from the converging stream lines.

Figure 4 shows the distribution of the scalar concentration at $t = 5\,000$ [s] released from the point source located at $x = -10$ [km] and $y = 1\,000 \sim 1\,200$ [m]. The stream of the scalar concentration is pulled lower behind the mountain due to the downward wind, but it ascends again as the flow changes its direction upward and is transported downstream in a wave-like manner. The concentration diffuses slightly as it passes over the mountain, as is seen from the diffused image of the concentration streak.

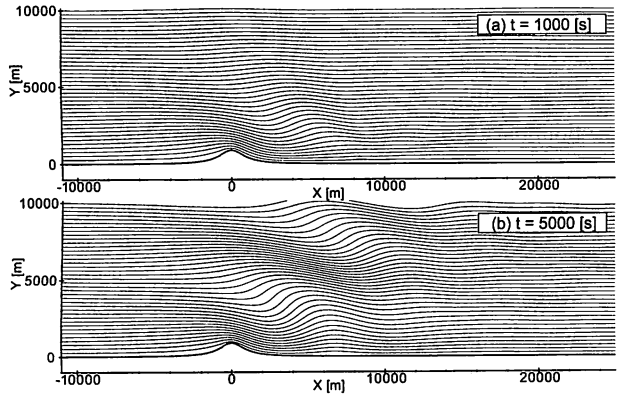

Fig. 2 Stream lines in the one-layer model for $Fr = 1.0$. (a) $t = 1\,000$ [s], (b) $t = 5\,000$ [s]

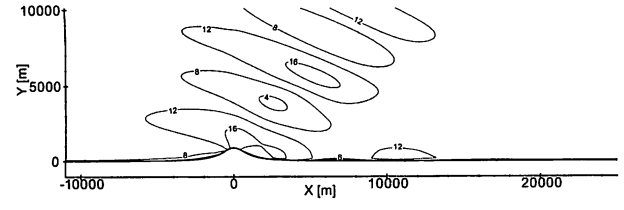

Fig. 3 Horizontal velocity for $Fr = 1.0$ at $t = 5\,000$ [s]

Figure 5 shows the ground scalar concentration at $t = 5\,000$ [s]. The value is divided by the concentration C_s near the release point at $x = -9\,900$ [m] and $y = 1\,100$ [m]. The concentration rises behind the mountain, and the values are the order of 10^{-8}. The ground scalar concentration for $Fr = 0.75$ is typically of the order of 10^{-7}.

3.2 Two-layer model

According to Scorer[10),(11)], in the region where the Scorer parameter, l, defined by

$$l = \frac{N}{U} \tag{8}$$

decreases with height, mountain waves cannot propagate in the upward direction. As a consequence they are trapped in the lower layer, where the Scorer parameter l is a non-decreasing number. The trapped mountain waves produce long and intensive wave trains, thus it is conceivable that they might diffuse the scalar concentration more efficiently than non-trapped mountain waves. For simplification, we employ a two-layer model in which the density gradient changes abruptly at an altitude of 11 km. Figure 6 shows the profiles of the background density ρ_B. In the upper layer, $d\rho_B/dy$ is set to 0 which makes $l = 0$.

Figure 7 (a) and (b) shows the horizontal velocity for $Fr = 0.75$ at $t = 2\,500$ and $5\,000$ [s], respectively. Mountain waves propagate obliquely upward with time as in the one-

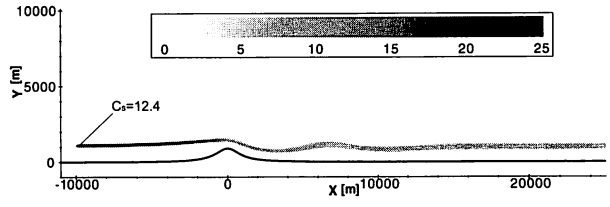

Fig. 4 Scalar concentration for $Fr = 1.0$ at $t = 5\,000$ [s]

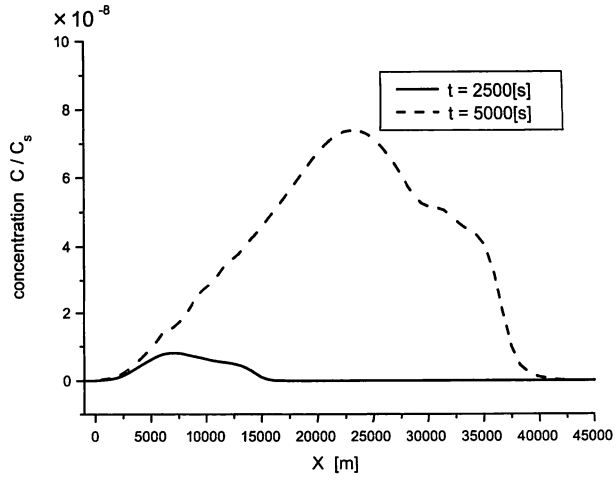

Fig. 5 Ground scalar concentrations for $Fr = 1.0$ at $t = 2\,500$ [s] ($C_s = 13.2$) and $t = 5\,000$ [s] ($C_s = 12.4$)

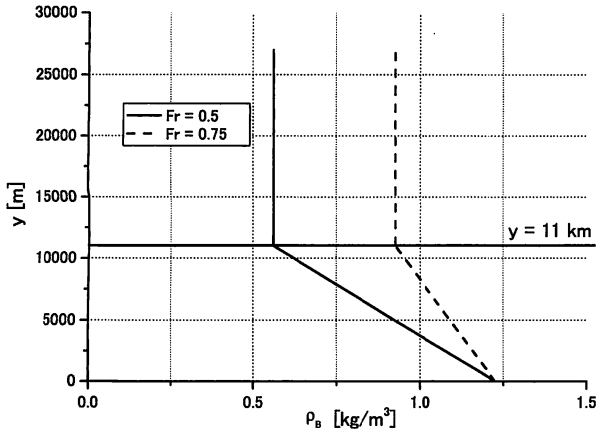

Fig. 6 Density profiles in the two-layer model

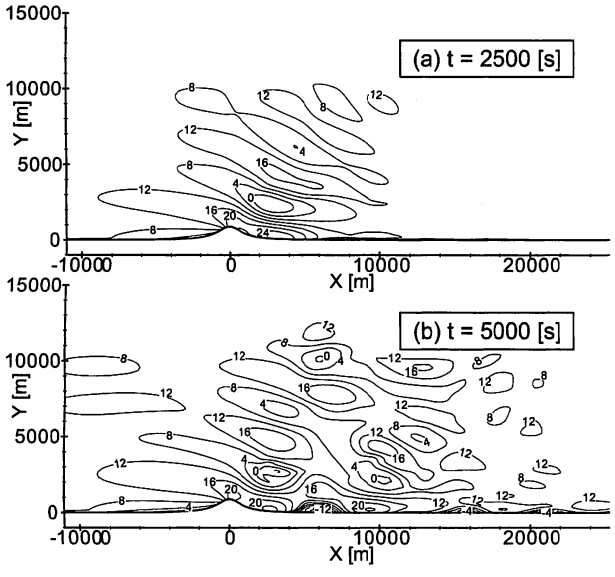

Fig. 7 Reflection of mountain waves at the interface of the two-layers ($Fr = 0.75$). (a) $t = 2\,500$ [s], (b) $t = 5\,000$ [s]

layer model, but when the waves reach the interface of the two layers, they reflect back into the lower atmosphere, and at $t = 5\,000$ [s] the flow field develops a net-like structure. It should be also noted that there are regions where the horizontal velocity has negative values on the ground on the leeward side of the mountain. They are recirculation regions known as rotors[7),(12)].

In Figs. 8 and 9 we show the flow field and the scalar concentration for $Fr = 0.75$ and 0.5 at $t = 5\,000$ [s], respectively

- $Fr = 0.75$

Mountain waves grow strongly and breaking waves, as well as rotors, are visible behind the mountain. A strong rotor is generated at around $x = 6$ [km] and relatively weak ones at around $x = 16$ [km] and 21 [km]. The scalar concentration released at the height $y = 1\,000 \sim 1\,200$ [m] reaches the ground and diffuses rapidly behind the rotors. On the other hand, the scalar concentration released at $y = 2\,000 \sim 2\,200$ [m] diffuses downstream of the mountain at around $x = 10$ [km], corresponding to the region where developing waves start to break.

- $Fr = 0.5$

In Fig. 9 (a), the mountain waves are even stronger than those for $Fr = 0.75$, and wave-breaking regions are observed at $y = 4$ [km] and 7 [km]. Rotors develop at $x = 8$ [km], 13 [km] and 18 [km]. As for $Fr = 0.75$, the scalar concentration released at $y = 1\,000 \sim 1\,200$ [m] reaches the ground and diffuses strongly behind the rotors, and the one from $y = 2\,000 \sim 2\,200$ [m] is trapped into a wave-breaking region in the air and accumulates there.

Figure 10 shows the ground scalar concentration when released at $y = 1\,000 \sim 1\,200$ [m] corresponding to Fig. 5 obtained from the one-layer model. The concentrations on the ground for $Fr \geq 1.0$ are negligible compared with those for $Fr = 0.75$ and 0.5. The leading edge of the concentration rise for $Fr = 0.75$ is observed at about

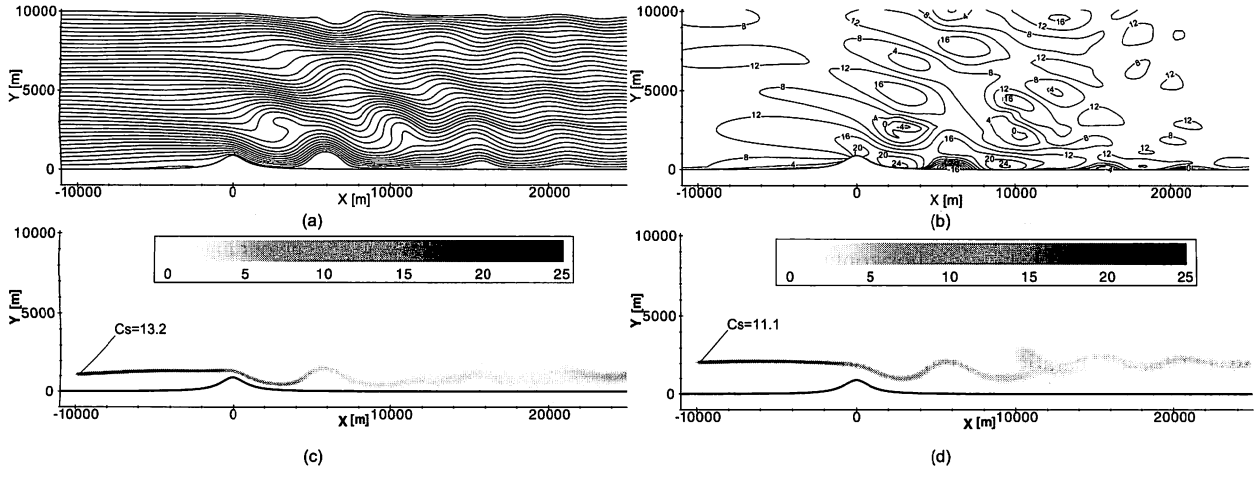

Fig. 8 Flow field and scalar concentration streak for $Fr = 0.75$ at $t = 5\,000$ [s], (a) Stream line, (b) Horizontal velocity, (c) Scalar concentration released from $y = 1\,000 \sim 1\,200$ [m], (d) $y = 2\,000 \sim 2\,200$ [m]

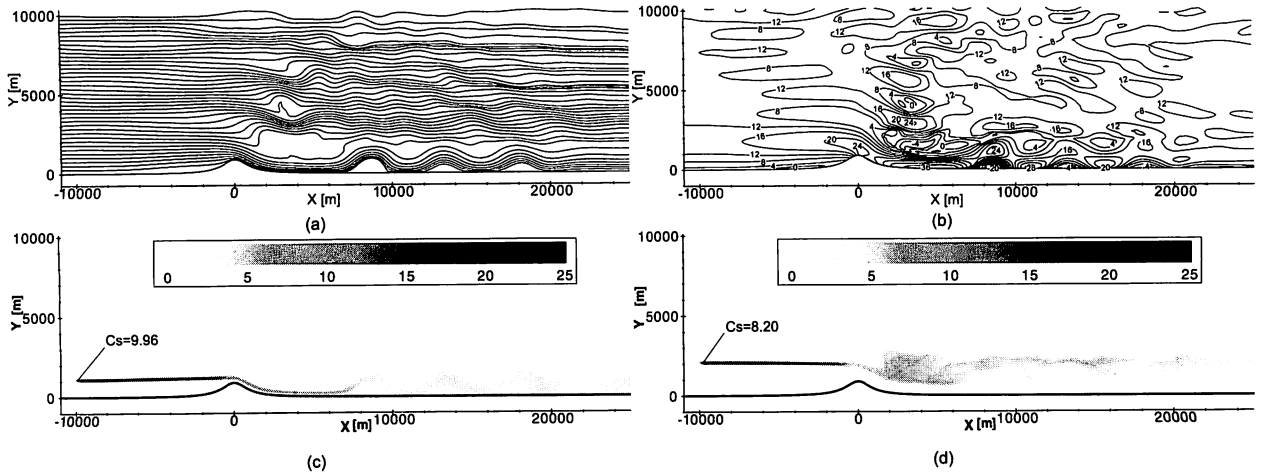

Fig. 9 Flow field and scalar concentration streak for $Fr = 0.5$ at $t = 5\,000$ [s], (a) Stream line, (b) Horizontal velocity, (c) Scalar concentration released from $y = 1\,000 \sim 1\,200$ [m], (d) $y = 2\,000 \sim 2\,200$ [m]

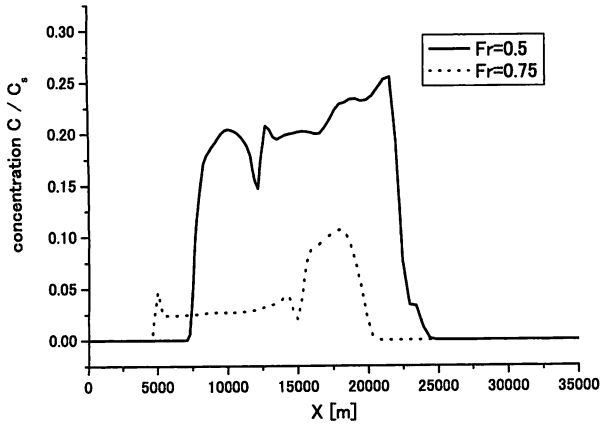

Fig. 10 Ground scalar concentrations from the two-layer model, with two different Froude numbers

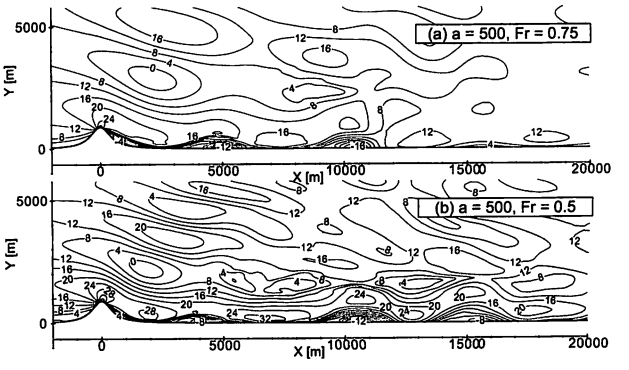

Fig. 11 Horizontal velocity contour lines for $a = 500$ [m] at $t = 5\,000$ [s], with two different Froude numbers (a) $Fr = 0.75$, (b) $Fr = 0.5$

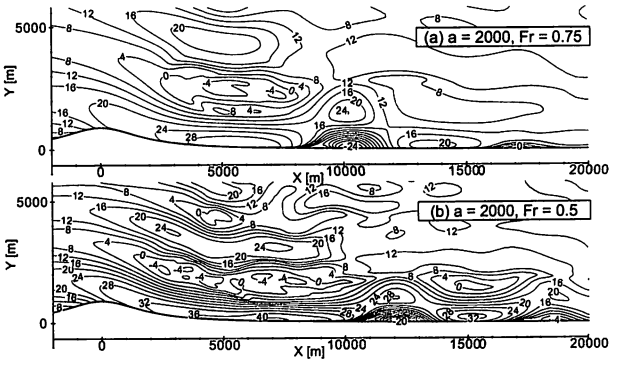

Fig. 12 Horizontal velocity contour lines for $a = 2\,000$ [m] at $t = 5\,000$ [s], with two different Froude numbers (a) $Fr = 0.75$, (b) $Fr = 0.5$

$x = 4$ [km] and the location corresponds to the front of the rotor as seen in Fig. 8 (a). The concentration drops at about 20 [km], corresponding to a termination of the 3rd weak rotor at $x = 21$ [km] in Fig. 8 (a). The concentration for $Fr = 0.5$ also rises at the front of the first rotor and decreases at the end of the third rotor. From the above observation, it can be said that rotors generated by mountain waves have a significant impact on the falling and diffusion of the scalar concentration at high altitude.

3.3 Effect of the mountain width

Figures 11 and 12 show the horizontal velocity when the mountain width is shortened to $a = 500$ [m] or extended to $a = 2\,000$ [m]. When $a = 500$ [m] and $Fr = 0.75$ (Fig. 11 (a)), a separation region behind the mountain is clearly visible with a negative value for the horizontal velocity, while for $Fr = 0.5$ the separation is somewhat suppressed and a region of stronger wind covers the down slope. This trend has been also reported by previous numerical studies[7),13)]. When $a = 2\,000$ [m] and $Fr = 0.75$, separation does not occur and the flow is parallel to the down slope behind the mountain. When $Fr = 0.5$, the flow structure is essentially unaltered, although the rotors develop more strongly. In general, it is known that mountain width affects the leeward flow separation structure in the stratified fluid[14)]. For instance, when the mountain width, A_d (where $A_d = 2a$), is short and $NA_d/U = lA_d < \pi$, sepa-

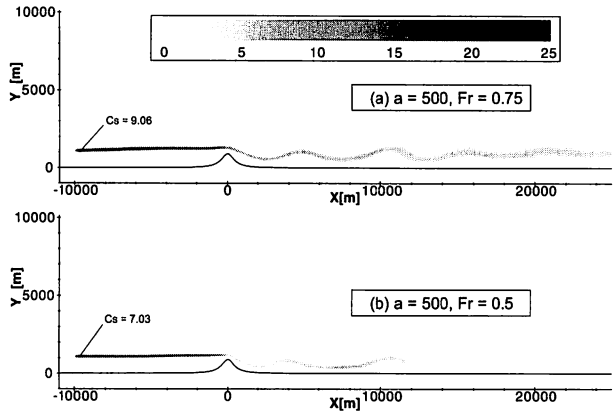

Fig. 13 Scalar concentration streak when it is released at $y = 1\,000 \sim 1\,200$ [m] with $a = 500$ [m], for two different Froude numbers, (a) $Fr = 0.75$, (b) $Fr = 0.5$

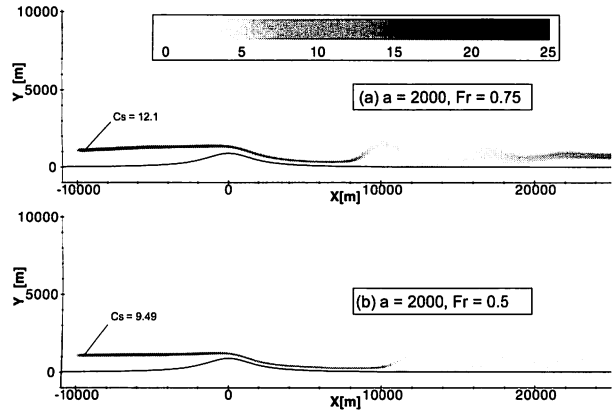

Fig. 14 Scalar concentration streak released at $y = 1\,000 \sim 1\,200$ [m] with $a = 2\,000$ [m], for two different Froude numbers, (a) $Fr = 0.75$, (b) $Fr = 0.5$

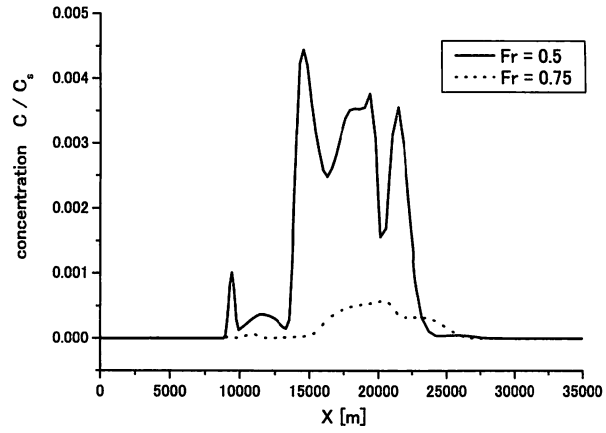

Fig. 15 The ground scalar concentration with $a = 500$ [m], for two different Froude numbers

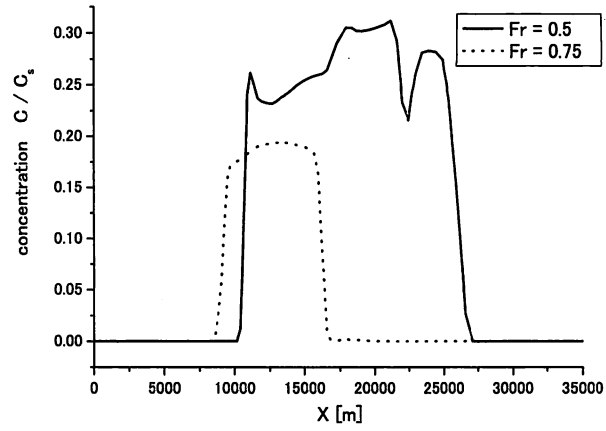

Fig. 16 The ground scalar concentration with $a = 2\,000$ [m], for two different Froude numbers

ration occurs behind the mountain. On the other hand, for $NA_d/U \geq \pi$, the separation is suppressed and the rotors are generated on the leeward side. These characteristics are reproduced in the present simulation.

Figures 13 and 14 show the distribution of scalar concentration released at $y = 1\,000 \sim 1\,200$ [m]. The scalar concentration for $a = 500$ [m] and $Fr = 0.75$ goes around the separation region behind the mountain, but when $Fr = 0.5$ it goes along the down slope and starts diffusing in the rotor regions. When $a = 2\,000$ [m] the scalar concentration is drawn closer to the down slope and diffuses more quickly in the rotor regions. The ground scalar concentration is shown in Figs. 15 and 16. The concentration rises in rotor regions as mentioned in section 3.2, but it is much higher for $a = 2\,000$ [m] than for $a = 500$ [m]. Hence, it is concluded that the mountain width has a significant effect on the overall transport of scalar concentration, and that the development of rotors is particularly important for defining a mechanism for falling high-altitude dust.

4. Conclusion

In this paper, we examined the effect of mountain waves on the transport of Yellow Sand by employing an unsteady two-dimensional numerical model for the density-stratified flow over a mountain.

In the one-layer model, where the Scorer parameter, l, is constant over the entire domain, mountain waves develop behind the topographical ridge and it is shown that the high altitude scalar concentration is pulled towards the ground. However, the rise in ground scalar concentration is found to be negligibly small. In the two-layer model, on the other hand, mountain waves reflect at the interface between the two layers, and are trapped and intensified in the lower atmosphere. Under $Fr = 0.75$ rotors are produced on the ground and high ground scalar concentrations are observed in the rotor regions. It is also shown that the concentrations increase as the atmosphere stabilizes. Therefore, there is a good possibility that Yellow Sand at high altitudes is pulled towards the ground and subsequently scattered due to the presence of the rotors. The topography has also a great influence on rotor strength, which intensifies for larger mountain width.

We have mainly focused in this work on the relationship between mountain waves and their effect on the trans-

port of Yellow Sand, and hence the effect of turbulence has not been our primary concern. Turbulence probably has, however, a significant influence on the behavior of Yellow Sand once it is pulled down into the atmospheric boundary layer, especially in the rotors. A more elaborate study of the turbulent diffusion in the rotors may be needed to predict more precisely the amount of dust that actually falls on the ground.

Acknowledgements

This work was supported by the 21st-Century COE Program of Kanazawa University "Environmental Monitoring and Prediction of Long and Short-Term Dynamics of Pan-Japan Sea Area". We would also like to thank Dr. Michael Vynnycky for his careful reading and correction of our paper.

References

(1) Sakai, T., Shibata, T., Kwon, S.A., Kim, Y.S., Tamura, K. and Iwasaka, Y., Free Tropospheric Aerosol Backscatter, Depolarization Ratio, and Relative Humidity Measured with the Raman Lidar at Nagoya in 1994–1997: Contributions of Aerosols from the Asian Continent and the Pacific Ocean, Atmos. Environ., Vol.34 (2000), pp.431–442.

(2) Uno, I., Amano, H., Emori, S., Kinoshita, K., Matsui, I. and Sugimoto, N., Trans-Pacific Yellow Sand Transport Observed in April 1998: A Numerical Simulation, J. Geophy. Res., Vol.106, No.D16 (2001), pp.18 331–18 344.

(3) In, H.J. and Park, S.U., A Simulation of Long-Range Transport of Yellow Sand Observed in April 1998 in Korea, Atmos. Environ., Vol.36 (2002), pp.4173–4187.

(4) Kai, K., Okada, Y., Uchino, O., Tabata, I., Nakamura, H., Takasugi, T. and Nikaidou, Y., Lidar Observation and Numerical Simulation of a Kosa (Asian Dust) over Tsukuba, Japan during the Spring of 1986, J. Meteor. Soc. Japan., Vol.66 (1988), pp.457–472.

(5) Lilly, D.K. and Zipser, E.J., The Front Range Windstorm of 11 January 1972 — A Meteorological Narrative, Weatherwise, Vol.25 (1972), pp.56–63.

(6) Iwagawa, M., Kawamura, T. and Shirayama, S., Numerical Simulation of Advection and Diffusion of the Smoke in Stratified Flow, Theo. Appl. Mech., Vol.48 (1999), pp.339–348.

(7) Uchida, T. and Ohya, Y., Numerical Study of Stably Stratified Flows over a Two-Dimensional Hill in a Channel of Finite Depth, Fluid Dyn. Res., Vol.29, No.4 (2001), pp.227–250.

(8) Utanohara, Y., Kimura, S. and Kiwata, S., Two-Dimensional Numerical Simulation of Yellow Sand Transport with Mountain Wave in Stably Stratified Atmosphere, Proc. 19th Symp. on CFD, C5-4, CD-ROM, (in Japanese), (2005).

(9) Trochkine, D., Iwasaka, Y., Matsuki, A., Zhang, D. and Osada, K., Aircraft Borne Measurements of Morphology, Chemical Elements, and Number-Size Distributions of Particles in the Free Troposphere in Spring over Japan: Estimation of Particle Mass Concentrations, J. Arid Land Stud., Vol.11, No.4 (2002), pp.327–335.

(10) Scorer, R., Theory of Waves in the Lee of Mountains, Quart. J. Roy. Meteor. Soc., Vol.75 (1949), pp.41–56.

(11) Durran, D.R., Mountain Waves, Mesoscale Meteorology and Forecasting, Edited by Ray, P.S., (1986), pp.472–492, Amer. Meteor. Soc.

(12) Doyle, J.D. and Durran, D.R., Recent Developments in the Theory of Atmospheric Rotors, Bull. Amer. Meteor. Soc., Vol.85 (2004), pp.337–342.

(13) Uchida, T. and Ohya, Y., Three-Dimensional Numerical Simulation of Stably Stratified Flows over a Two-Dimensional Hill-Stratification Effect on an Unsteady Separated and Reattaching Flow, Nagare, (in Japanese), Vol.22 (2003), pp.65–78.

(14) Baines, P.G., Topographic Effects in Stratified Flows, (1995), Cambridge University Press.